frontiers in Forests and Global Change

METHODS
published: 04 June 2019
doi: 10.3389/ffgc.2019.00025

High-Resolution *in vivo* Imaging of Xylem-Transported CO_2 in Leaves Based on Real-Time ^{11}C-Tracing

Michiel Hubeau[1], Michael R. Thorpe[2], Jens Mincke[1,3], Jasper Bloemen[1], Ingvar Bauweraerts[1], Peter E. H. Minchin[4], Veerle De Schepper[1], Filip De Vos[5], Christian Vanhove[3], Stefaan Vandenberghe[3] and Kathy Steppe[1]*

[1] Laboratory of Plant Ecology, Faculty of Bioscience Engineering, Ghent University, Ghent, Belgium, [2] Research School of Biology, The Australian National University, Canberra, ACT, Australia, [3] MEDISIP-INFINITY, Faculty of Engineering and Architecture, Ghent University-IMEC, Ghent, Belgium, [4] Te Puke Research Centre, New Zealand Institute for Plant and Food Research Limited, Auckland, New Zealand, [5] Laboratory of Radiopharmacy, Ghent University, Ghent, Belgium

OPEN ACCESS

Edited by:
*Anna Sala,
University of Montana, United States*

Reviewed by:
*Adam Coble,
Oregon Department of Forestry, United States
John Marshall,
Swedish University of Agricultural Sciences, Sweden*

***Correspondence:**
*Kathy Steppe
kathy.steppe@UGent.be*

Specialty section:
This article was submitted to Forest Ecophysiology, a section of the journal Frontiers in Forests and Global Change

Received: *06 December 2018*
Accepted: *13 May 2019*
Published: *04 June 2019*

Citation:
Hubeau M, Thorpe MR, Mincke J, Bloemen J, Bauweraerts I, Minchin PEH, De Schepper V, De Vos F, Vanhove C, Vandenberghe S and Steppe K (2019) High-Resolution in vivo Imaging of Xylem-Transported CO_2 in Leaves Based on Real-Time ^{11}C-Tracing. Front. For. Glob. Change 2:25. doi: 10.3389/ffgc.2019.00025

Plant studies using the short-lived isotope ^{11}C to label photosynthate via atmospheric carbon dioxide (CO_2), have greatly advanced our knowledge about the allocation of recent photosynthate from leaves to sinks. However, a second source for photosynthesis is CO_2 in the transpiration stream, coming from respiration in plant tissues. Here, we use *in vivo* tracing of xylem-transported $^{11}CO_2$ to increase our knowledge on whole plant carbon cycling. We developed a new method for *in vivo* tracing of xylem-transported CO_2 in excised poplar leaves using ^{11}C in combination with positron emission tomography (PET) and autoradiography. To show the applicability of both measurement techniques in visualizing and quantifying CO_2 transport dynamics, we administered the tracer via the cut petiole and manipulated the transport by excluding light or preventing transpiration. Irrespective of manipulation, some tracer was found in main and secondary veins, little of it was fixed in minor veins or mesophyll, while most of it diffused out the leaf. Transpiration, phloem loading and CO_2 recycling were identified as mechanisms that could be responsible for the transport of internal CO_2. Both ^{11}C-PET and autoradiography can be successfully applied to study xylem-transported CO_2, toward better understanding of leaf and plant carbon cycling, and its importance in different growing conditions.

Keywords: *Populus canadensis*, ^{11}C (carbon-11), isotope, radiotracer, positron emission tomography (PET), positron autoradiography, xylem CO_2 transport

INTRODUCTION

Within trees, the flow of carbon between organs and metabolic processes or storage pools plays an important role for the overall plant carbon cycle (Litton et al., 2007; Epron et al., 2012). Since the main pathway for carbon transport considered in research on carbon allocation is the phloem, which distributes sugars to sink tissues, a multitude of techniques have been designed to monitor the fate of assimilated sugars. In particular, isotopic techniques, either based on tracing of stable or unstable isotopes, have recently gained increased interest (Epron et al., 2012; Bahn et al., 2013; Hubeau and Steppe, 2015).

Recent research has shown that CO_2 derived from above- and belowground respiration is transported with the transpiration stream in trees (Teskey et al., 2008, 2017; Aubrey and Teskey, 2009; Bloemen et al., 2013b, 2016a; Steppe et al., 2015), thereby representing a second important transport pathway of the plant carbon cycle. Gaseous CO_2 in solution is in equilibrium with other carbonate species. It reacts with water to form carbonic acid (H_2CO_3) which, in turn, can dissociate to bicarbonate (HCO_3^-) and carbonate (CO_3^{2-}) by losing one or two hydrogen ions (H^+), respectively. The concentration of these species in solution is depending on the pH with the dominant form being CO_2 and bicarbonate for the reported xylem pH (4.5–7.4) of woody species (Teskey et al., 2008). A fraction of the respired CO_2 is fixed (Stringer and Kimmerer, 1993; McGuire et al., 2009; Bloemen et al., 2013a, 2015; Steppe et al., 2015; Tarvainen et al., 2017; Wittmann and Pfanz, 2018), potentially contributing to the amount of carbon available for metabolic processes. Bloemen et al. (2013b) have pulse-labeled the transpiration stream of field-grown poplar trees using the stable isotope ^{13}C to trace respired CO_2 transport at the tree level, finding that 3–17 % of the tracer was immobilized in the tree, including 0.3–2% in the leaves. Similar experiments have been performed at the level of branch (McGuire et al., 2009; Bloemen et al., 2013a) and leaf (Bloemen et al., 2015).

The destructive nature of ^{13}C-tissue analysis and its limited temporal resolution currently hinder our understanding of the importance of xylem-transported CO_2 in plant carbon cycling. Studies investigating the dynamics of xylem-transported CO_2 are therefore scarce. Here, we investigate whether short-living radioactive isotopes can help (Hubeau and Steppe, 2015). ^{11}C has a half-life of 20.4 min and has been exploited mostly for dynamic studies aiming to understand the controls on distribution of recent photosynthates (Minchin and Thorpe, 2003). Several methodologies can be used. Using scintillation detectors, with radiation shielding to delineate regions of interest (ROI), a range of phenomena has been studied concerning phloem physiology, for example in root apices (Pritchard et al., 2004), roots (Farrar et al., 1995), properties of the long-distance transport pathway (Troughton et al., 1974; Minchin and Thorpe, 1984), in leaves (Pickard et al., 1993), and in reproductive organs (Roeb and Britz, 1991; Thorpe et al., 1993). The low spatial resolution of this method is not a problem for measurement of long-distance tracer transport since the flow at the boundary from one contiguous region to another can be inferred (e.g., Minchin and Thorpe, 2003). With positron radiography, complementary snapshots can show tracer distribution at a much higher spatial resolution (Pritchard et al., 2004), which has also been demonstrated by our group (Bloemen et al., 2015; Epila et al., 2018; Mincke et al., 2018; Hubeau et al., 2019b). Other transported compounds can be studied after appropriate radiosynthesis, such as methyl jasmonate (Thorpe et al., 2007), carbon tetrachloride (Ferrieri et al., 2006), 2-[18F]fluoro-2-deoxy-D-glucose (Ferrieri et al., 2012). With PET imaging, it is possible to combine good spatial resolution (0.7–4 mm) with high time resolution (5–60 s), and ROIs can be generated after data collection, both for dynamic studies (Jahnke et al., 2009) and to help choose tissue for chemical analysis (Dirks et al., 2012). However, studies using ^{11}C have been uncommon, because the isotope's short half-life means that transport from the production facility to the plant biology laboratory needs to take less than about 30 min. Until recently, few laboratories have had a production facility nearby, but that is becoming more common, with short-lived isotopes (mostly ^{18}F and ^{11}C) being produced for many medical imaging facilities where PET scanners are used for both clinical diagnosis and biomedical research (Karve et al., 2015). Also, the 20 min half-life of ^{11}C limits its use to short-term processes, in contrast to the longer-lived carbon isotope ^{14}C (half-life of 5,730 years). On the positive side, ^{11}C-tracing allows an *in vivo* observation of tracer movement, which has led to significant research progress in topics such as phloem sectoriality (De Schepper et al., 2013), unloading characteristics (Jahnke et al., 2009), leakage-retrieval of photoassimilates along the transport pathway (Thorpe and Minchin, 1991), phloem functioning under changing climate regimes (Hubeau et al., 2019a) and carbon allocation to root and fruit parts (Jahnke et al., 2009; Wang et al., 2014). Importantly, non-invasive measurements allow dynamic aspects of a process to be studied, and ^{11}C therefore provides a powerful tool to reveal the mechanisms of physiological processes (Minchin and Thorpe, 2003; Jahnke et al., 2009; Bühler et al., 2011; Hubeau et al., 2019a). Here, we demonstrate another use of this tool, studying CO_2 transport in the xylem.

To this end, we designed a new method that allows *in vivo* monitoring of xylem CO_2 transport in leaves based on ^{11}C-tracing and PET in combination with autoradiography. In nearly all previous plant studies, ^{11}C has been supplied to the plant as airborne $^{11}CO_2$, with the aim of gaining insight into photoassimilate production and transport, and phloem functioning. Here, we utilized a PET scanner to dynamically trace $^{11}CO_2$ in excised leaves that had received aqueous $^{11}CO_2/H^{11}CO_3^-$ buffer via the cut petiole to investigate and unravel the interplay between xylem architecture and xylem-derived CO_2 as a substrate for photosynthesis in leaves (Stringer and Kimmerer, 1993; Bloemen et al., 2015). The ^{11}C-PET technique was complemented by ^{11}C-positron autoradiography, giving a snapshot in time with a much higher spatial resolution. Simple manipulations were performed to highlight both the high amount of process-level knowledge that can be extracted through this technique, and also the applicability of both imaging techniques. The overall goal was to shed light on the interplay and importance of CO_2 flows in a leaf after arrival in leaf xylem: convection in xylem, diffusion within the leaf and photochemical fixation. To that end, we performed two manipulation experiments regarding photosynthesis and gas exchange within one half of a leaf, hypothesizing that (i) excluding light would stop CO_2 fixation in the dark region, and (ii) stopping gas exchange and thus transpiration within a region would prevent the local convective movement of xylem CO_2 resulting in no fixation. The aims of this study were therefore to indicate: (i) the feasibility of ^{11}C-PET for plants using a small-animal PET scanner, (ii) the research potential of ^{11}C-PET to trace short-term transport processes in plants, (iii) the complementarity of ^{11}C-PET and autoradiography, and

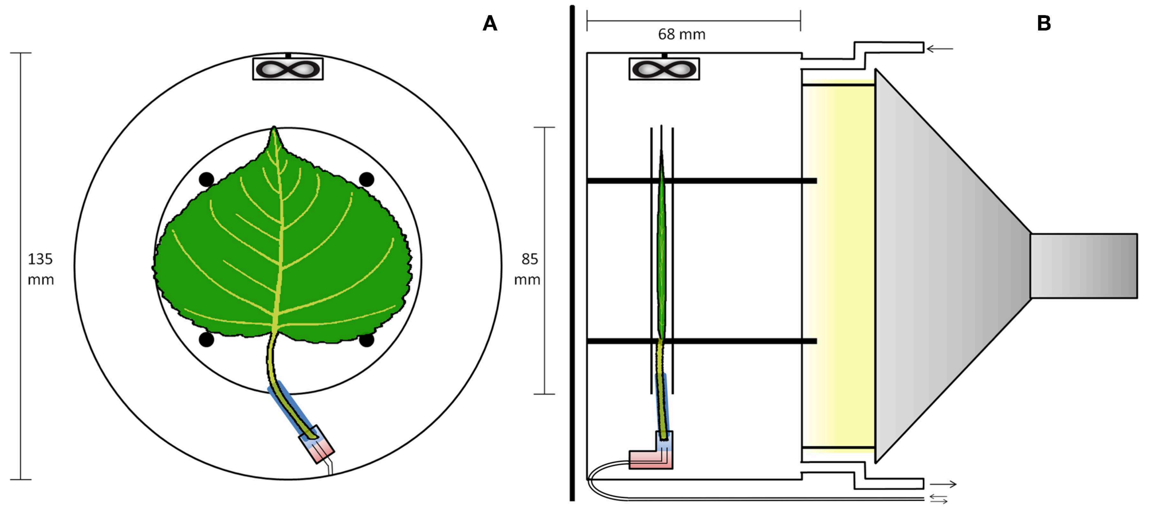

FIGURE 1 | PET imaging setup with the leaf inside the cuvette. **(A)** Transverse view of the cuvette. An elastic polysiloxane sleeve (blue) seals the petiole to the plastic elbow junction (rectangle), and two-component epoxy (red) seals two (0.6 mm inner diameter) tubes to the junction for delivering solutions, as in **Figure 2**. **(B)** Sagittal view of the cuvette. The leaf is sandwiched between two planar nylon meshes (not shown) woven between four posts, while two 4 mm plexiglas discs (apparent in both **A,B**) are placed to trap positrons that escape the leaf. The fan ensures good mixing of air flowing through the cuvette. The light source was outside the scanner, attached to the cuvette using three metal screws.

(iv) new insights into xylem-derived CO_2 fixation by the use of diagnostic treatments.

MATERIALS AND METHODS

Plant Material

For this study, 20 cm long poplar cuttings (*Populus* × *canadensis* Moench "Robusta") were planted early April 2012 in 4-L pots containing a commercial potting mixture (DCM, Grobbendonk, Belgium) and slow-releasing fertilizer (Basacote Plus 6M, Compo Benelux nv, Deinze, Belgium), and were grown within a growth chamber at the Faculty of Bioscience Engineering, Ghent University, Belgium. Temperature was controlled day and night at 25°C and photosynthetically active radiation (PAR) was provided with densely packed fluorescent lamps (TLD 80, Philips Lighting NV, Eindhoven) from 8 h until 22 h. The cuttings were watered every 2 days. The leaves used for the experiments were selected to be similar in age and in size (∼22 cm^2).

Experimental Setup and ^{11}C-Labeling

Since ^{11}C is a short-living isotope, the experiment was performed close to a cyclotron (18/9 MeV, IBA, Belgium). The proximity allowed quick transport of the produced ^{11}C to the INFINITY imaging lab of Ghent University, Ghent, Belgium. There, $^{11}CH_4$ produced from the (p, α) nuclear reaction in the cyclotron on a nitrogen target was oxidized in a synthetic train to yield $^{11}CO_2$ as described by Landais and Finn (1989). The captured $^{11}CO_2$ gas was immediately bubbled through "carrier solution" (50 mM KOH with 500 mM TRIS buffer at pH 6.4) giving ^{11}C-labeled CO_2 solution, which was subsequently supplied to the cut petiole of an excised leaf. Under these conditions 90% of the ^{11}C is present as HCO_3^- and 10% as CO_2 in a dynamic equilibrium.

Real-time ^{11}C-tracing was performed on an excised leaf in a plexiglass cylindrical airtight labeling cuvette (135 mm inner diameter and 68 mm depth, **Figure 1**) in an open system. The cuvette was kept just below atmospheric pressure to avoid leakage of $^{11}CO_2$ out of the leaf cuvette by generating air flow (1.5 L min^{-1}) with a pump at the end of the pathway (model 2-Wisa, Hartmann and Braun, Frankfurt am Main, Germany) (**Figure 2**). Before entering a dew point generator (Li-610, Li-COR, Lincoln, TE, USA), air first entered a 50 L buffer vessel. Relative humidity (RH) and temperature of the air entering the cuvette were controlled using the dew point generator. RH and air temperature, averaged (± SD) over the labeling periods, were 28.4 ± 0.8 % and 30.2 ± 0.6°C, respectively. A small fan (20 × 20 × 7.5 mm; Sunon, Kaohsiung, Taiwan) was installed close to the air inlet, so as to stir and direct airflow over both surfaces of the leaf (**Figure 1**). For radiation safety, air exiting the leaf cuvette was bubbled through KOH solution (50 mM) to remove $^{11}CO_2$, before passing to the pump. A fiber-optic light source (Model FL-4000, Walz Mess und Regeltechnik, Effeltrich, Germany) provided PAR of 926 μmol m^{-2} s^{-1} at the leaf surface (**Figure 1B**).

Because of the isotope's rapid decay, the labeling system (**Figure 2**) was designed to give a minimal time-delay for the tracer to enter the petiole after labeling. For the junction between petiole and its supply tubing we used a plastic elbow. Two supply tubes (inner diameter of 0.6 mm), one for continuous supply of carrier solution, the other for delivery of tracer solution, were sealed to one end of the junction using two-component glue (Loctite, Düsseldorf, Germany). For each experiment, a 25 mm long cylindrical sleeve was molded around the petiole of the selected leaf, using 2-component polysiloxane elastomer (Xantopren, Heraeus Kulzer, GmbH, Hanau, Germany). The

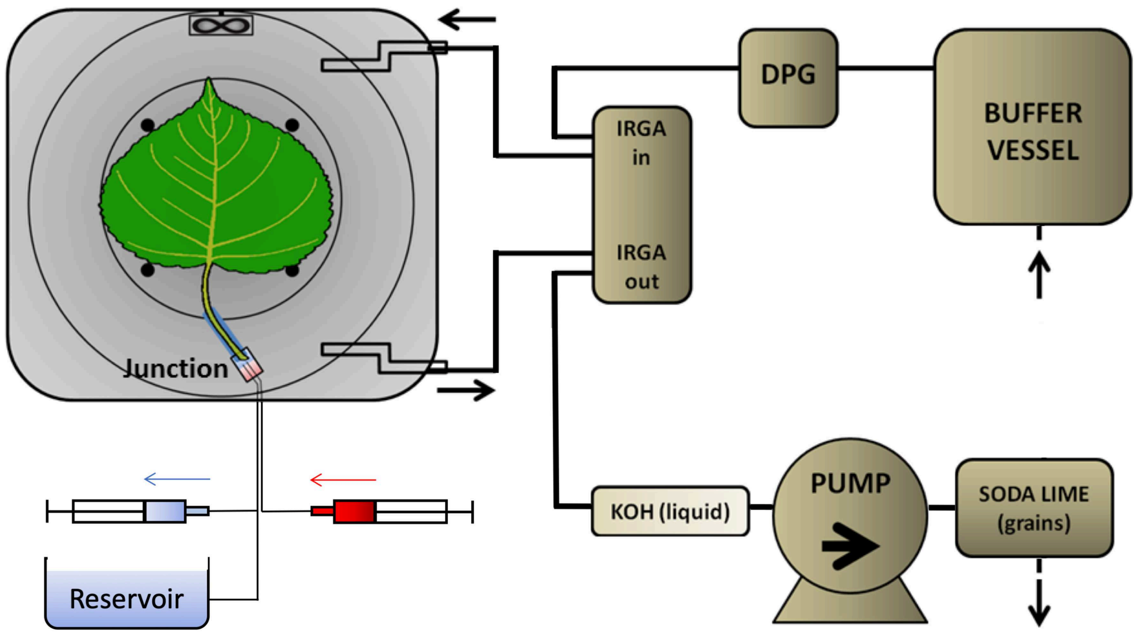

FIGURE 2 | Flow schedule of the PET imaging setup. The PET detectors (dark-gray around the leaf cuvette) were shielded from most of the tubing in which $^{11}CO_2$ was likely present. Ambient air was drawn by a pump that was placed near the end of the pathway to prevent leaks of radioactive gas. The air passed through a 30-L buffer vessel, a dew point generator (DPG), to and from the leaf cuvette via two infra-red gas analyser channels (IRGA), to a KOH trap. As a final safety measure, all air passed from the pump through a granular soda lime trap. The excised leaf received non-labeled solution from a reservoir open to the atmosphere, which was large enough to maintain a constant pressure at the leaf. Tracer was delivered to a small volume in the junction from the 3-mL syringe (red) while simultaneously withdrawing unlabelled solution from the junction into the other syringe (blue). Solution from the reservoir then continued to supply the leaf xylem.

sleeve formed a seal around the petiole and could be inserted into the elbow fitting. About 2 h before labeling, with the junction already full of carrier solution and connected to the reservoir, the petiole was cut under water, to prevent air entry. The sleeved petiole was then inserted into the junction, and the leaf was then mounted in the gas-exchange cuvette. Pressure in the junction was held atmospheric by adjusting the height of the reservoir's liquid, forestalling leaks. For labeling, two 3-ml syringes were used to avoided pressure fluctuations and leaks (**Figure 2**). Simultaneously, 2 mL labeled carrier solution (7.4 MBq) was delivered from the "hot" syringe, replacing the same volume of solution being withdrawn from the junction into a syringe on a T-junction in the supply tubing. Pressure continued thereby to be atmospheric. After that, carrier solution from the reservoir continued to supply the leaf through the junction, which had a volume of about 0.5 mL. For trouble-shooting, arrival of tracer to the leaf petiole was assessed through the PET scanner's real-time decay event counter. In order to reduce random coincident events in the scanner, the syringe of ^{11}C labeled solution, together with the water source and most of the tubing, were shielded from the PET detector using stackable lead blocks.

^{11}C-Imaging Techniques

^{11}C-imaging is based on the radioactive decay of ^{11}C, which occurs with a half-time of 20.4 min. ^{11}C decays to ^{11}B through emission of a positron (β^+-radiation), with a maximum energy of 0.96 MeV, and a neutrino (υ_e) (Equation 1) (Bailey et al., 2005):

$$^{11}C \rightarrow {}^{11}B + \beta^+ + \upsilon_e \tag{1}$$

This positron moves along a random path, suffering collisions by which its energy reduces until it can annihilate with an electron (**Figure 3**). In water—and in tissue—that zig-zag path is about 5 mm long, but the radial range for an ^{11}C-nuclide is less, 1.1 mm, and 90 % of the positrons stop within 2.2 mm (Cho et al., 1975; Jødal et al., 2012). Annihilation results in two high-energy photons, which move off in opposite directions (**Figure 3**) (Bailey et al., 2005). These photons (γ-rays) each have an energy of 511 keV and can easily penetrate thick layers of plant tissues: the thickness of tissue (and water) that is required to reduce the intensity of a beam by one half is ~7 cm (Bailey et al., 2005). In PET, these γ-rays are registered, whereas in autoradiography, mainly the positrons are detected.

^{11}C-PET Analysis

The PET scanner (LabPET8, TriFoil Imaging, Chatsworth, CA, USA) used in our experiment is based on several LGSO ($Lu_{0.4}Gd_{1.6}SiO_5$:Ce) and LYSO ($Lu_{1.9}Y_{0.1}SiO_5$:Ce) scintillation crystals assembled side-by-side and read out by avalanche photodiodes, sensitive to a determined range of photon energy and placed along a cylindrical surface. When an ^{11}C-atom decays inside this cylinder, and the positron-electron annihilation results into two γ-photons, two opposing detectors register an incoming

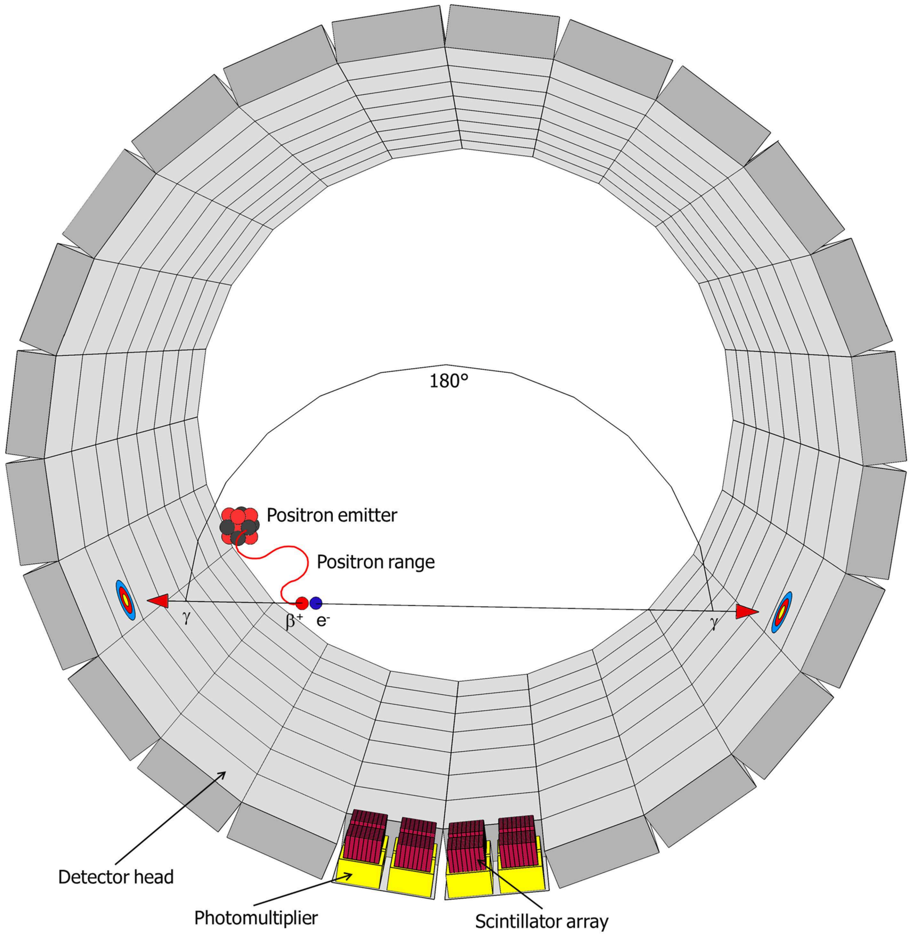

FIGURE 3 | Schematic representation of a decaying radionuclide emitting a positron (β^+), which will collide with an electron (e^-) after traveling a certain distance (positron range) resulting in the annihilation with the emission of two gamma-rays (γ) in opposite direction. This radiation will be detected in the detector head by a scintillator and the resulting signal is enhanced by photomultipliers (after Hubeau and Steppe, 2015 with the permission of Copyright Clearance Center).

photon. Dedicated software filters such co-occurring photons, indicative of a decay event, and generates spatial probability graphs of all decay events over a certain time frame (**Figure 3**). Technical advances (such as the time-of-flight PET or enhanced reconstruction algorithms) are continuously increasing spatial and temporal resolution of these scanners. A significant portion of ^{11}C-positrons can escape the leaf lamina and therefore reduce sensitivity and spatial resolution (Alexoff et al., 2011; Partelová et al., 2016). The leaf was therefore additionally fixed between two circular plexiglass plates (diameter of 85 mm and thickness of 2.5 mm) spaced 0.5 cm from each other, improving the sensitivity, but reducing the resolution of the images. These plates were attached concentrically to the cuvette by four plastic screws (**Figure 1**).

LabPET software version 1.12.1 (TriFoil Imaging, Chatsworth, CA, USA) was used to reconstruct the PET data with a temporal resolution of 5 min. The exponential decline in activity, due to decay of the radioactive isotope, is accounted for by the software. To avoid ambiguity, we use the term "tracer" to mean "decay-corrected activity," reserving the term "activity" for the detected events. The resulting output was analyzed using AMIDE (http://amide.sourceforge.net, GNU General Public License version 2.0 (GPLv2)). Voxel tracer values were normalized to the maximum voxel value in the time-series. The PET images map average tracer density within a slice of specified thickness, centered on the leaf. In this work, we used a 30 mm thickness, enclosing both leaf and discs, to ensure that all annihilations were accounted for. A background ROI outside the leaf was used to subtract a background count-rate. PET data was recorded for 60 and 100 min for control and treated leaves, respectively.

^{11}C-Autoradiography Setup

At the end of the experiment, the cuvette was taken out of the PET scanner. After removing the elastic sleeve from the petiole and the leaf from the cuvette, the leaf was wrapped in transparent cellophane to prevent contamination of the imaging plate while radioactivity was imaged by positron autoradiography, exposing the adaxial side of the leaf by direct contact with an imaging phosphor plate for 5 min, after which the plate was digitally scanned (Cyclone Plus Phosphor imager, Perkin Elmer, Waltham, MA, USA) and quantified using OptiQuant version 5.0 (Perkin Elmer, Waltham, MA, USA) (Mincke et al., 2018; Hubeau et al., 2019b). Images are not mutually corrected for radioactivity.

Manipulation Experiments

To test the robustness of our setup and to demonstrate the applicability of both techniques (PET and autoradiography) to visualize and quantify dynamics of internal CO_2 transport and fixation, experiments were conducted on three different leaves: (i) not treated; (ii) half-shaded, with one half of the leaf lamina (including midrib) shaded by covering half of the plexiglass plate closest to the light source (**Figure 1B**), aiming to minimize photosynthetic activity; (iii) half-greased, with one half of the leaf greased on both the abaxial and adaxial surfaces using translucent petrolatum (i.e., petroleum jelly or Vaseline) before the leaf was installed in the labeling cuvette to prevent gas exchange.

RESULTS

Microclimate

The microclimate of each experiment is characterized by an average vapor pressure deficit of 3.02 ± 0.12, 2.70 ± 0.19, and 2.51 ± 0.04 kPa in the non-treated, shaded, and greased leaves, respectively. Average transpiration rates of the non-treated, shaded, and greased leaf were 1.811 ± 0.905, 0.946 ± 0.473, and 1.437 ± 0.479 mmol s^{-1} m^{-2}, respectively, and photosynthetic rates averaged around 0.041 ± 0.012, 0.028 ± 0.008 and 0.023 ± 0.003 μmol CO_2 s^{-1}, respectively. The half-shaded and half-greased leaves thus transpired 48 % and 21 % less water, and assimilated 33 and 42% less carbon, respectively, compared to the control leaf.

Images

The PET image sequence of tracer density for each leaf (**Figures 4a–c**) shows tracer moving from the petiole through the leaf to gradually reveal both the main vein and basal secondary veins in the non-treated regions of all leaves. Little was visible in the shaded leaf-half (**Figure 4b**), but surprisingly considerable amounts of tracer moved into the greased leaf-half (**Figure 4c**). The PET image sequences showed that most tracer was not fixed, as it declined steeply after passing a maximum, showing loss of tracer, presumably by outgassing via stomata.

Autoradiographs show more detail of the activity that remained in each leaf after the PET image sequence (**Figure 5**). The labeling pattern of non-treated regions was similar, with activity extending all the way to the perimeter of the leaves in minor veins, but little to none in the mesophyll. Tracer density in the veins declined with distance from the petiole (Bloemen et al., 2015). In the shaded region, all minor veins were labeled, but density declined toward the leaf perimeter much more in comparison with the non-treated half. In the half-greased leaf, some tracer was visible over the greased region confirming that tracer had moved into that region, but hardly any tracer reached the leaf perimeter. The labeling pattern of the non-greased region was more uniform and intense compared to exposed regions in the other leaves, suggesting that tracer was fixed in minor veins and even mesophyll. However, replications are needed to further confirm our results.

Tracer Dynamics

More details of tracer dynamics were derived from the time-series of tracer within specified regions (regions are shown in **Figure 4**). Profiles of tracer within each leaf and its two halves (**Figures 6A–C**) showed that most of the tracer entering a leaf was in due course lost from it by the end of the experiments (in particular observable in the longer experiments of 100 min). It is also obvious that movement was much slower in the half-shaded leaf than in either the non-treated or half-greased leaves. Tracer concentration within each ROI (L) reached a peak around 25, 45, and 20 min for the non-treated, half-shaded and half-greased, respectively. After that, the tracer in each ROI was well-described by a single exponential with a time constant of approximately 45 min.

DISCUSSION

^{11}C-Based Tracing of Xylem CO_2 Transport and Fixation

So far, the role of xylem CO_2 transport in plants has been mainly studied using the unstable ^{14}C (Stringer and Kimmerer, 1993; Hibberd and Quick, 2002) and the stable ^{13}C (McGuire et al., 2009; Bloemen et al., 2013a,b) isotopes. However, good dynamic measurements cannot be made with those isotopes because destructive sampling is necessary, although recently it has been recognized that Bremsstrahlung radiation from ^{14}C is energetic enough to be useful (Black et al., 2012). Here, we have demonstrated that xylem CO_2 transport in excised tree leaves can be traced continuously and *in vivo* when PET-based ^{11}C-analysis is used, mimicking the transport and fixation of that CO_2. It is important to gain better insights into the movement and fixation of respired CO_2 to develop a comprehensive framework on carbon cycling and its implications in leaves and plants.

Most of the ^{11}C-label applied at the leaf petiole was distributed throughout the leaf via the leaf veins. Water and sugar transport mainly occur through the main vein because of the heterobaric vein structure in poplar, which causes a strong compartmentalization of the leaf mesophyll by bundle sheath extensions (McClendon, 1992). Most of the immobilized tracer was found in the petiole and veins, suggesting that xylem-transported $^{11}CO_2$ was being fixed in or very near to the vasculature. These findings correspond with the results of McGuire *et al.* (2009) where branches were allowed to transpire water enriched with $^{13}CO_2$. In that study, 35% (SE = 2.4) of the label was fixed via woody tissue photosynthesis, with little moving into the petioles and leaf laminae. Here, that immobilization of CO_2 near the xylem could also explain the decline in tracer with distance from the source, as shown by Bloemen et al. (2015) from similar data.

Tracer in all leaf regions followed an exponential decline after reaching a maximum, suggesting a common cause, the time-variation of tracer entering the petiole. The long time

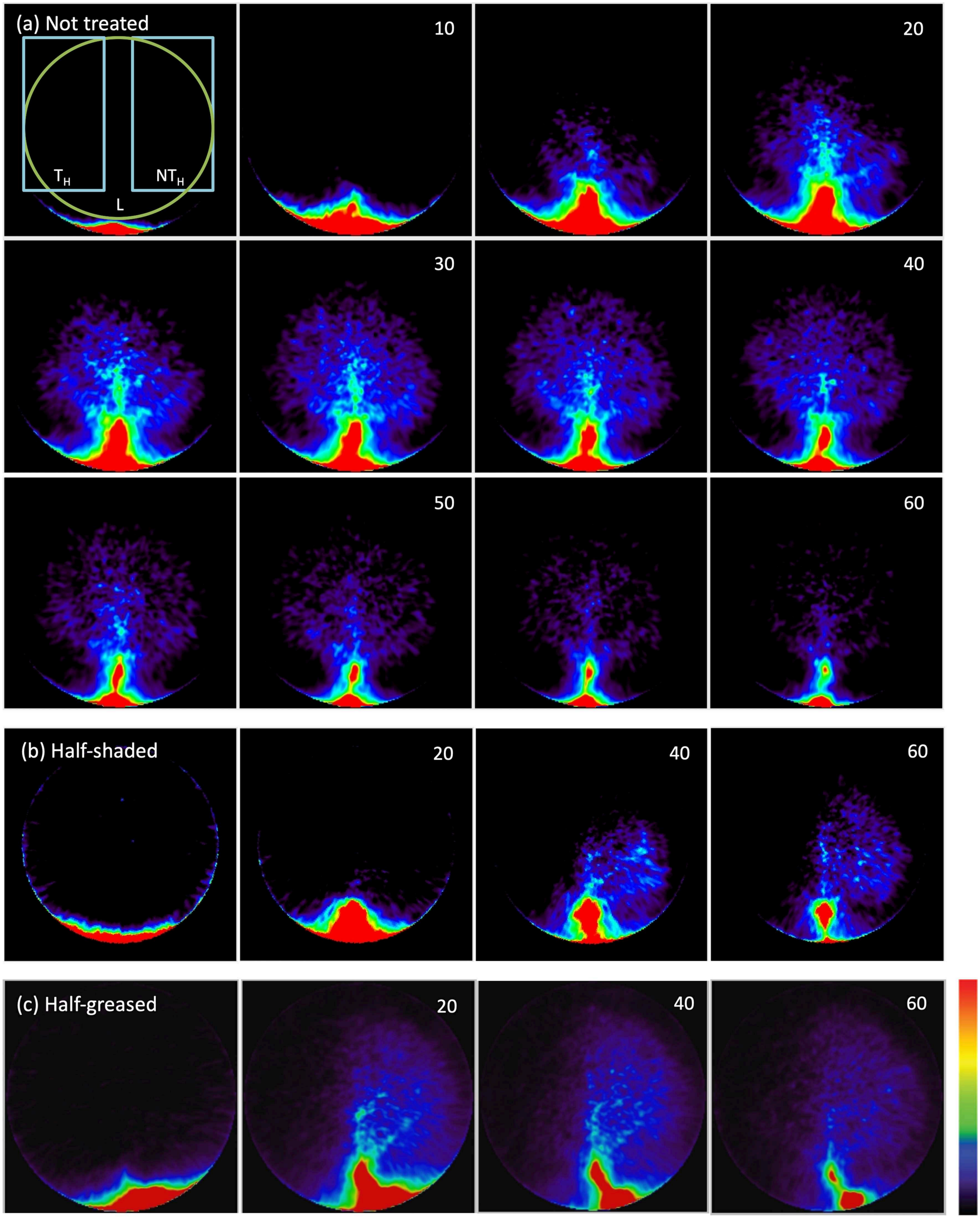

FIGURE 4 | ^{11}C PET images of a **(a)** non-treated leaf, **(b)** half-shaded leaf, **(c)** half-greased leaf. Numbers in the upper right corner show time (minutes) after the start of labeling. Each image shows the decay-corrected sum of all decay events (tracer) in the last 5-min **(a)** or 20-min **(b,c)** interval. The first PET image of **(a)** displays the ROIs of the leaf (L), treated (T_H) and non-treated (NT_H) halves that were used to create time-series (**Figure 6**) for all conditions (non-treated, shading and grease). Colors varying from black to red represents no to high tracer as indicated by the color bar.

constant of that decline (about 45 min), due to dilution of the administered tracer by unlabeled carrier solution from the reservoir, dominated tracer dynamics. Hereby obscuring the dynamics of tracer exiting the leaf, we can conclude that exit dynamics was much faster than the above 45 min (since the data are well–described by only one exponential).

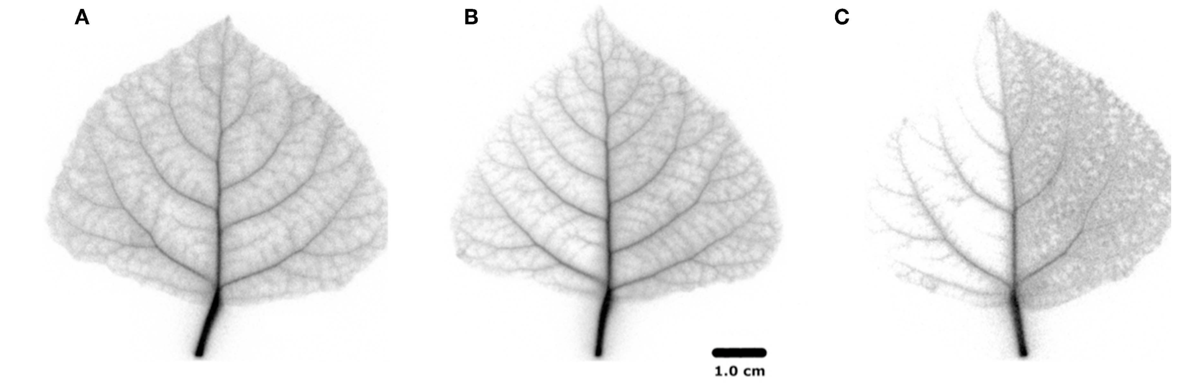

FIGURE 5 | ^{11}C positron autoradiograms for the three differently-treated leaves; **(A)** non-treated leaf, **(B)** half-shaded leaf, **(C)** half-greased leaf.

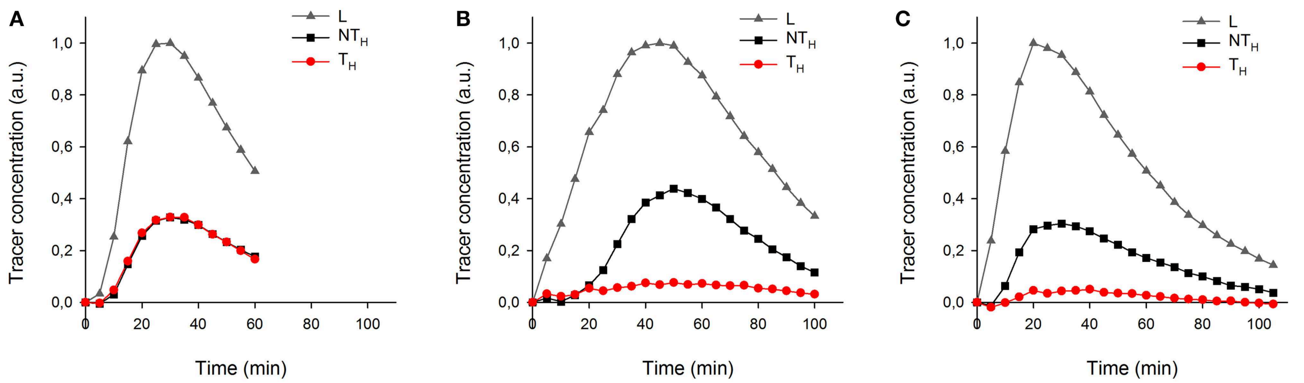

FIGURE 6 | The temporal tracer (decay-corrected activity) profiles of the ROIs L, T_H and NT_H (as indicated on **Figure 4a**) for all conditions: **(A)** non-treated leaf, **(B)** half-shade leaf, and **(C)** half-greased leaf. Tracer was summed per 5 min for each ROI.

The exponential tails of the time-series showed no asymptote greater than zero, indicating that a very large fraction of the xylem-borne CO_2 diffused out of the leaf, presumably through stomata, and helped by the slightly acidic pH of our xylem sap. Nevertheless, the autoradiographs, having higher sensitivity, showed that some CO_2 from the xylem was indeed fixed.

To test the applicability of the proposed ^{11}C-labeling for studying xylem CO_2 transport dynamics, we manipulated xylem CO_2 transport rates in one leaf half using shading or grease treatments while keeping the other leaf half untreated as reference. Both PET and autoradiographic image analyses showed differences in xylem CO_2 transport between leaf halves, with a substantially lower amount of label in the treated leaf half (T_H) as compared with the untreated one (NT_H) (**Figures 6B,C**). Interestingly, the amount of tracer measured in secondary veins on the autoradiographs was hardly influenced by the treatments (**Figure 5**). Further transport to minor veins and mesophyll was however clearly reduced by both treatments. Shading half of the leaf surface reduced transpiration by half compared to the control leaf. With half the transpiration and half the leaf shaded, transpirational water flow into the leaf reduced, reducing the amount and flow velocity of ^{11}C-labeled solution into the unshaded half. Accumulation of ^{11}C in the shaded half (**Figure 5B**) indicated that water was also flowing into this region despite the exclusion of light. This can be explained by limited transpiration under dark conditions comparable to nocturnal transpiration, which is not uncommon and known to occur in poplar (Caird et al., 2007; Dawson et al., 2007; Zeppel et al., 2014). Transpiration in the darkened leaf half will even be stronger compared to a nocturnal leaf as atmospheric conditions in the cuvette were drier than during a typical night.

The treatment with grease stops leaf transpiration (as utilized for example by Gribaudo et al. (2001) and Shackel et al. (1990)) and was therefore expected to stop local convective movement of $^{11}CO_2$ into the greased leaf half. According to the cohesion-tension theory, the driving force for water transport disappears in the absence of transpiration, but interestingly we observed that the ^{11}C-label did enter the secondary veins of the greased leaf half, although import into the minor veins and mesophyll was hampered (**Figure 5C**). Diffusion within the secondary veins cannot be the explanation as CO_2 would have been able to diffuse only 0.06 mm in 1 h, given the diffusion coefficient of CO_2 in water of only 1.6×10^{-9} m^2 s^{-1} (Nobel, 1999; Steppe et al., 2007), and leaves of poplar are heterobaric, hindering any gas transport. Four mechanisms for some ongoing xylem inflow to that region are suggested, although in the first three cases the inflow would be transient. First, after evaporation stopped, the greased region may not have fully hydrated before tracer labeling. Second, any ongoing phloem loading and transport of sugars from the leaf lamina toward the petiole would generate a small counter-flow of water in the xylem (Tanner and Beevers, 2001; Windt et al., 2006) explaining the ^{11}C-label in the greased leaf half (**Figure 5C**). Third, in the presence of light, some locally respired CO_2 in cells near the secondary veins might have been photosynthesised into sugars that generated a transient influx of water to restore cell turgor, drawing water from petiole to leaf veins (Nikinmaa et al., 2013; Stroock et al., 2014). Fixation of respired CO_2 has indeed been shown to occur in bundle sheath cells, surrounding the vascular bundle (Griffiths et al., 2013). Fourth, it may be that the grease did not completely stop evaporation of the leaf-half, since the transpiration rate of the half-greased leaf reduced by only 20%, not 50%.

Why Should We Measure Xylem CO_2 Transport in Plants?

Within trees, the transport of locally respired CO_2 via the transpiration stream represents an additional pathway of carbon transport, counter flowing the phloem transport of recent photosynthates from leaves to sink tissues (Teskey et al., 2008). Aubrey and Teskey (2009) measured xylem CO_2 transport at the bottom of *Populus deltoides* trees as an estimate of internally transported belowground respired CO_2 and estimated that half of belowground respired CO_2 was transported internally instead of diffusing into the soil environment thereby showing that current soil CO_2 efflux-based methods underestimate the autotrophic component of soil respiration. Bloemen et al. (2013a,b) used stable isotope ^{13}C labeling approaches to trace respired CO_2 in field-grown trees and detached branches, respectively. They observed that the applied ^{13}C label was assimilated in different tissues, indicating that xylem-transported CO_2 can be fixed and hence contribute to tree biomass. At leaf level, such fixation occurred in the petiole mainly (Bloemen et al., 2013a,b). However, a fraction of xylem-transported CO_2 was also transported in the leaf vasculature and into the leaf mesophyll (Bloemen et al., 2015). This way, photosynthetically active cells lying adjacent to the transpiration stream might be fed with carbon from a different source than the atmospheric one (Hibberd and Quick, 2002; Griffiths et al., 2013). In our study, we also observed patterns in the half-shaded and half-greased leaf that point to the importance of fixing internally cycled CO_2. A substantial amount of internally transported CO_2 remained in the vasculature where it could be fixed by cells adjacent to the veins. With PET, it is not possible to detect in what molecular structure ^{11}C is present (e.g., dissolved CO_2 or ^{11}C-sucrose). Dirks *et al.* (2012) therefore used a set-up with a combination of ^{11}C and ^{13}C labeling to acquire both dynamic tracer images and molecular structure information (from NMR analysis). Janacek et al. (2009) showed that photosynthesis near veins, presumably utilizing xylem-transported CO_2, is important for plant fitness, by comparing untreated plants with plants with silenced chlorophyll synthase in the veins, which showed a marked reduction in growth. This process of CO_2 recycling is receiving increasingly more attention as more evidence accumulates to support this as an important mechanism to sustain both carbon supply and hydraulic functioning under drought conditions (Schmitz et al., 2012; Cernusak and Cheesman, 2015; Steppe et al., 2015; Vandegehuchte et al., 2015; Bloemen et al., 2016b; De Baerdemaeker et al., 2017; Chen et al., 2018).

The Power of Imaging ^{11}C-Labeled Compounds in Plant Research

The potential of ^{11}C-positron emission tomography (^{11}C-PET) in plant studies remains largely untapped (Hubeau and Steppe, 2015). In past studies, ^{11}C-tracing has been used to study the transport speed of phytomolecules such as plant hormones (e.g., methyl jasmonate in Thorpe et al., 2007) and photoassimilates (Kikuchi et al., 2008), and ^{11}C-imaging has been used to visualize the phloem pathway for part of the plant (Kawachi et al., 2006; Jahnke et al., 2009; De Schepper et al., 2013; Hubeau et al., 2019a) or the entire plant (Kawachi et al., 2011). The acquired tracer profiles can be implemented in mathematical models to study sugar loading, sugar translocation, radial sugar leakage and sugar unloading (Bühler et al., 2011, 2014; Minchin, 2012; Hubeau et al., 2019a).

Those studies that have applied radio-isotopes to trace xylem CO_2 transport used almost exclusively the long-living ^{14}C isotope. For instance, Stringer and Kimmerer (1993) allowed excised leaves to transpire dissolved ^{14}C label. Using autoradiography, they confirmed that xylem CO_2 was transported in the leaf vasculature to different leaf sections. In addition, Stringer and Kimmerer (1993) performed light manipulation experiments and observed that a large amount of the ^{14}C label applied to the leaf diffused into the atmosphere. Our group performed ^{11}C-based autoradiography to analyse CO_2 assimilation which resulted in a static autoradiogram (Bloemen et al., 2015; Epila et al., 2018; Mincke et al., 2018; Hubeau et al., 2019b). In this study, our PET $^{11}CO_2$ imaging method provides the first continuous *in vivo* data on xylem CO_2 transport, allowing us to study the transport pathways of xylem CO_2 transport in plants at high temporal resolution. With a relatively simple set of manipulation experiments we could already see detailed differences between treatments and gathered detailed spatial and temporal carbon distribution maps. Due to their fine spatial and temporal resolution, and the fast decay of the activity, the PET images appear noisy and mottled (for the 7.4 MBq activity we used), but signal to noise was markedly improved for time-series of ROI content (**Figure 6**), integrating large volumes of the PET images.

The high energy (511 keV) of the photons resulting from ^{11}C-decay penetrates tissue and allows *in vivo* detection of tracer in thick plant tissues. This would allow our observations of xylem CO_2 transport at leaf level to be expanded to branch or tree level, as performed already to study photosynthate allocation in the phloem of small trees (Jahnke et al., 1998; De Schepper et al., 2013). Also, since ^{11}C is a short-living isotope with a half-life of 20.4 min, it allows repeated pulse labeling on the same plant so that changes in transport properties can be monitored. A next step would be to design a set-up in which the imaged leaf remains attached to the tree branch or stem (Hubeau and Steppe, 2015), although higher ^{11}C-activity than the 7.4 MBq that we used in our experiment would be necessary in order to resolve different tissues. For thicker samples, such as woody stems, the high energy of γ-rays in PET would give useful results, using phantoms to account for attenuation.

CONCLUSION

Our results highlight the potential importance of internal CO_2 for the plant in the production of local sugars in the vasculature with an important impact on water transport in the study leaves. With ^{11}C-PET we were able to extract valuable information, both qualitative (high-resolution images) and dynamic (tracer profiles), on the movement of internal CO_2. A combination of PET with positron autoradiography, which took little additional effort, resulted in even more information on the distribution of carbon inside a leaf under different conditions. This yields promising outlooks for future experiments, potentially in combination with related techniques such as micro-CT for structural information, SPECT for functional information with heavier isotopes and MRI to visualize and quantify water flow in xylem and phloem.

AUTHOR CONTRIBUTIONS

MT, CV, SV, and KS designed the research. MT, JB, IB, and CV performed the experiments. MH, MT, JM, JB, and IB analyzed and interpret the data. MH, MT, JM, JB, IB, and KS wrote the manuscript. All authors read and edited the manuscript before publication.

FUNDING

This project was supported by a starting grant from the Scientific Research Foundation Flanders (FWO) by research program G.0319.13N to KS, FD, and SV and SB fellowship 1S37716N granted to JM. The authors also wish to thank the Flanders Innovation & Entrepreneurship Agency for the Ph.D. funding granted to MH (141660), and the Special Research Fund (BOF) of Ghent University for the postdoctoral funding granted to VD (01P02712) and for MT's Visiting Foreign Researcher grant (BOF11/VBO/019-MT).

ACKNOWLEDGMENTS

The authors wish to thank Philip Deman and Geert Favyts of the Laboratory of Plant Ecology, Ghent University, for their enthusiastic technical support, and to Jan Courtyn from the cyclotron team at UZ Ghent to make the production of $^{11}CO_2$ possible.

REFERENCES

Alexoff, D. L., Dewey, S. L., Vaska, P., Krishnamoorthy, S., Ferrieri, R., Schueller, M., et al. (2011). PET imaging of thin objects: measuring the effects of positron range and partial-volume averaging in the leaf of Nicotiana tabacum. *Nucl. Med. Biol.* 38, 191–200. doi: 10.1016/j.nucmedbio.2010.08.004

Aubrey, D. P., and Teskey, R. O. (2009). Root-derived CO_2 efflux via xylem stream rivals soil CO_2 efflux. *New Phytol.* 184, 35–40. doi: 10.1111/j.1469-8137.2009.02971.x

Bahn, M., Lattanzi, F. A., Hasibeder, R., Wild, B., Koranda, M., Danese, V., et al. (2013). Responses of belowground carbon allocation dynamics to extended shading in mountain grassland. *N. Phytolol.* 198, 116–126. doi: 10.1111/nph.12138

Bailey, D., Karp, S., and Surti, S. (2005). "Physics and instrumentation in PET," in *Positron Emission Tomography*, eds D. Bailey, D. Townsend, P. Valk, M. Maisey (Berlin: Springer), 13–39.

Black, M. Z., Minchin, P. E. H., Gould, N., Patterson, K. J., and Clearwater, M. J. (2012). Measurement of Bremsstrahlung radiation for *in vivo* monitoring of ^{14}C tracer distribution between fruit and roots of kiwifruit (*Actinidia arguta*) cuttings. *Planta* 236, 1327–1337 doi: 10.1007/s00425-012-1685-z

Bloemen, J., Bauweraerts, I., De Vos, F., Vanhove, C., Vandenberghe, S., Boeckx, P., et al. (2015). Fate of xylem-transported ^{11}C- and ^{13}C-labeled CO_2 in leaves of poplar. *Physiol. Plant.* 153, 555–564. doi: 10.1111/ppl.12262

Bloemen, J., McGuire, M. A., Aubrey, D. P., Teskey, R. O., and Steppe, K. (2013a). Assimilation of xylem-transported CO_2 is dependent on transpiration rate but is small relative to atmospheric fixation. *J. Exp. Bot.* 64. 2129–2138. doi: 10.1093/jxb/ert071

Bloemen, J., McGuire, M. A., Aubrey, D. P., Teskey, R. O., and Steppe, K. (2013b). Transport of root-respired CO_2 via the transpiration stream affects aboveground carbon assimilation and CO_2 efflux in trees. *N. Phytol.* 197, 555–565. doi: 10.1111/j.1469-8137.2012.04366.x

Bloemen, J., Teskey, R. O., McGuire, M. A., Aubrey, D. P., and Steppe, K. (2016a). Root xylem CO_2 flux: an important but unaccounted-for component of root respiration. *Trees* 30, 343–352. doi: 10.1007/s00468-015-1185-4

Bloemen, J., Vergeynst, L. L., Overlaet-Michiels, L., and Steppe, K. (2016b). How important is woody tissue photosynthesis in poplar during drought stress? *Trees* 30, 63–72. doi: 10.1007/s00468-014-1132-9

Bühler, J., Huber, G., Schmid, F., and Blümler, P. (2011). Analytical model for long-distance tracer-transport in plants. *J. Theor. Biol.* 270, 70–79. doi: 10.1016/j.jtbi.2010.11.005

Bühler, J., von Lieres, E., and Huber, G. (2014). A class of compartmental models for long-distance tracer transport in plants. *J. Theor. Biol.* 341, 131–142. doi: 10.1016/j.jtbi.2013.09.023

Caird, M. A., Richards, J. H., and Donovan, L. A. (2007). Nighttime stomatal conductance and transpiration in C_3 and C_4 Plants. *Plant Physiol.* 143, 4–10. doi: 10.1104/pp.106.092940

Cernusak, L. A., and Cheesman, A. W. (2015). The benefits of recycling: how photosynthetic bark can increase drought tolerance. *N. Phytol.* 208, 995–997. doi: 10.1111/nph.13723

Chen, X., Gao, J., Zhao, P., McCarthy, H. R., Zhu, L., Ni, G., et al. (2018). Tree species with photosynthetic stems have greater nighttime sap flux. *Front. Plant Sci.* 9:30. doi: 10.3389/fpls.2018.00030

Cho, Z. H., Chan, J. K., Ericksson, L., Singh, M., Graham, S., MacDonald, N. S., et al. (1975). Positron ranges obtained from biomedically important positron-emitting radionuclides. *J. Nucl. Med.* 16, 1174–1176

Dawson, T. E., Burgess, S. S., Tu, K. P., Oliveira, R. S., Santiago, L. S., Fisher, J. B., et al. (2007). Nighttime transpiration in woody plants from contrasting ecosystems. *Tree Phys.* 27, 561–575. doi: 10.1093/treephys/27.4.561

De Baerdemaeker, N. J. F., Salomon, R. L., De Roo, L., and Steppe, K. (2017). Sugars from woody tissue photosynthesis reduce xylem vulnerability to cavitation. *N. Phytol.* 216, 720–727 doi: 10.1111/nph.14787

De Schepper, V., Bühler, J., Thorpe, M., Roeb, G., Huber, G., van Dusschoten, D., et al. (2013). ^{11}C-PET imaging reveals transport dynamics and sectorial plasticity of oak phloem after girdling. *Front. Plant Sci.* 4:200. doi: 10.3389/fpls.2013.00200

Dirks, R. C., Singh, M., Potter, G. S., Sobotka, L. G., and Schaefer, J. (2012). Carbon partitioning in soybean (*Glycine max*) leaves by combined ^{11}C and ^{13}C labeling. *N. Phytol.* 196, 1109–1121. doi: 10.1111/j.1469-8137.2012.04333.x

Epila, J., Hubeau, M., and Steppe, K. (2018). Drought effects on photosynthesis and implications of photoassimilate distribution in ^{11}C-labeled leaves in the African tropical tree species *Maesopsis eminii*. *Forests* 9 :109. doi: 10.3390/f9030109

Epron, D., Bahn, M., Derrien, D., Lattanzi, F. A., Pumpanen, J., Gessler, A., et al. (2012). Pulse-labelling trees to study carbon allocation dynamics: a review of methods, current knowledge and future prospects. *Tree Physiol.* 32, 776–798. doi: 10.1093/treephys/tps057

Farrar, J. F., Minchin, P. E. H., and Thorpe, M. R. (1995). Carbon import into barley roots: effects of sugars and relation to cell expansion. *J. Exp. Bot*. 46, 1859–1865. doi: 10.1093/jxb/46.12.1859

Ferrieri, A. P., Appel, H., Ferrieri, R. A., and Schultz, J. C. (2012). Novel application of 2-[18 F] fluoro-2-deoxy-d-glucose to study plant defenses. *Nucl. Med. Biol*. 39, 1152–1160. doi: 10.1016/j.nucmedbio.2012.06.005

Ferrieri, A. P., Thorpe, M. R., and Ferrieri, R. A. (2006). Stimulating natural defenses in poplar clones (OP-367) increases plant metabolism of carbon tetrachloride. *Int. J. Phytoremediat*. 8, 233–243. doi: 10.1080/15226510600846780

Gribaudo, I., Novello, V., and Restagno, M. (2001). Improved control of water loss from micropropagated grapevines (*Vitis vinifera* cv. Nebbiolo). *Vitis* 40, 137–140.

Griffiths, H., Weller, G., Toy, L. F., and Dennis, R. J. (2013). You're so vein: bundle sheath physiology, phylogeny and evolution in C3 and C4 plants. *Plant Cell Environ.* 36, 249–261. doi: 10.1111/j.1365-3040.2012.02585.x

Hibberd, J. M., and Quick, W. P. (2002). Characteristics of C_4 photosynthesis in stems and petioles of C_3 flowering plants. *Nature* 415, 451–454. doi: 10.1038/415451a

Hubeau, M., Mincke, J., Vanhove, C., Courtyn, J., Vandenberghe, S., and Steppe, K. (2019a). Plant-PET to investigate phloem vulnerability to drought in *Populus tremula* under changing climate regimes. *Tree Physiol.* 39, 211–221. doi: 10.1093/treephys/tpy131

Hubeau, M., Mincke, J., Vanhove, C., Gorel, A. P., Fayolle, A., Epila, J., et al. (2019b). ^{11}C-autoradiographs to image phloem loading. *Front. For. Glob. Change.* 2:20. doi: 10.3389/ffgc.2019.00020

Hubeau, M., and Steppe, K. (2015). Plant-PET scans: *in vivo* mapping of xylem and phloem functioning. *Trends Plant Sci.* 20, 676–685. doi: 10.1016/j.tplants.2015.07.008

Jahnke, S., Menzel, M. I., van Dusschoten, D., Roeb, G. W., Buhler, J., Minwuyelet, S., et al. (2009). Combined MRI-PET dissects dynamic changes in plant structures and functions. *Plant, J.* 59, 634–644. doi: 10.1111/j.1365-313X.2009.03888.x

Jahnke, S., Schlesinger, U., Feige, G. B., and Knust, E. J. (1998). Transport of photoassimilates in young trees of *Fraxinus* and *Sorbus*: measurement of translocation *in vivo*. *Bot. Acta* 111, 307–315. doi: 10.1111/j.1438-8677.1998.tb00714.x

Janacek, S. H., Trenkamp, S., Palmer, B., Brown, N. J., Parsley, K., Stanley, S., et al. (2009). Photosynthesis in cells around veins of the C3 plant *Arabidopsis thaliana* is important for both the shikimate pathway and leaf senescence as well as contributing to plant fitness. *Plant J.* 59, 329–343. doi: 10.1111/j.1365-313X.2009.03873.x

Jødal, L., Loirec, C. L., and Champion, C. (2012). Positron range in PET imaging: an alternative approach for assessing and correcting the blurring. *Phys. Med. Biol.* 57:3931. doi: 10.1088/0031-9155/57/12/3931

Karve, A. A., Alexoff, D., Kim, D., Schueller, M. J., Ferrieri, R. A., and Babst, B. A.,(2015). *In vivo* quantitative imaging of photoassimilate transport dynamics and allocation in large plants using a commercial positron emission tomography (PET) scanner. *BMC Plant Biol.* 15:273. doi: 10.1186/s12870-015-0658-3

Kawachi, N., Kikuchi, K., Suzui, N., Ishii, S., Fujimaki, S., Ishioka, N. S., et al. (2011). Imaging of carbon translocation to fruit using carbon-11-labeled carbon dioxide and positron emission tomography. *IEEE Trans. Nucl. Sci.* 58, 395–399. doi: 10.1109/TNS.2011.2113192

Kawachi, N., Sakamoto, K., Ishii, S., Fujimaki, S., Suzui, N., Ishioka, N. S., et al. (2006). Kinetic analysis of carbon-11-labeled carbon dioxide for studying photosynthesis in a leaf using positron emitting tracer imaging system. *IEEE Trans. Nucl. Sci*. 53, 2991–2997. doi: 10.1109/TNS.2006.881063

Kikuchi, K., Ishii, S., Fujimaki, S., Suzui, N., Matsuhashi, S., Honda, I., et al. (2008). Real-time Analysis of Photoassimilate Translocation in Intact Eggplant Fruit using $^{11}CO_2$ and a Positron-emitting Tracer Imaging System. *J. Jpn. Soc. Hortic. Sci*. 77, 199–205. doi: 10.2503/jjshs1.77.199

Landais, P., and Finn, R. (1989). On-line preparation of [^{11}C]carbon dioxide from [^{11}C]methane. *Int. J. Rad. Appl. Instrum*. 40, 265–266. doi: 10.1016/0883-2889(89)90161-5

Litton, C. M., Raich, J. W., and Ryan, M. G. (2007). Carbon allocation in forest ecosystems. *Global Change Biol*. 13, 2089–2210 doi: 10.1111/j.1365-2486.2007.01420.x

McClendon, J. H. (1992). Photographic survey of the occurence of bundle-sheath extensions in deciduous dicots. *Plant Physiol.* 99, 1677–1679. doi: 10.1104/pp.99.4.1677

McGuire, M. A., Marshall, J. D., and Teskey, R. O. (2009). Assimilation of xylem-transported ^{13}C-labelled CO_2 in leaves and branches of sycamore (*Platanus occidentalis,* L.). *J. Exp. Bot*. 60, 3809–3817. doi: 10.1093/jxb/erp222

Minchin, P. E. H. (2012). "Input-output analysis of phloem partitioning within higher plants," in *System identification, Environmental Modelling, and Control System Design,* eds L. Wang, H. Garnier (Berlin: Springer), 519–532.

Minchin, P. E. H., and Thorpe, M. R. (1984). Apoplastic phloem unloading in the stem of bean. *J. Exp. Bot*. 35, 538–550. doi: 10.1093/jxb/35.4.538

Minchin, P. E. H., and Thorpe, M. R. (2003). Using the short-lived isotope ^{11}C in mechanistic studies of photosynthate transport. *Funct. Plant Biol*. 30, 831–841. doi: 10.1071/FP03008

Mincke, J., Hubeau, M., Courtyn, J., Brans, B., Vanhove, C., Vandenberghe, S., et al. (2018). "Normalization of ^{11}C-autoradiographic images for semiquantitative analysis of woody tissue photosynthesis," in *Acta Hortic. 1222. ISHS 2018. Proceedings of the X International Workshop on Sap Flow,* eds L. S. Santiago and H. J. Schenk (Fullerton, CA), 35–41.

Nikinmaa, E., Höltt,ä, T., Hari, P., Kolari, P., Mäkel,ä, A., Sevanto, S., et al. (2013). Assimilate transport in phloem sets conditions for leaf gas exchange. *Plant Cell Environ*. 3, 655–669. doi: 10.1111/pce.12004

Nobel, P. S. (1999). *Physicochemical and Environmental Plant Physiology*. San Diego, CA: Academic Press.

Partelová, D., Horník, M., Lesný, J., Rajec, P., Kováč, P., and Hostin, S. (2016). Imaging and analysis of thin structures using positron emission tomography: thin phantoms and *in vivo* tobacco leaves study. *Appl. Radiat. Isot.* 115, 87–96. doi: 10.1016/j.apradiso.2016.05.020

Pickard, W. F., Minchin, P. E. H., and Thorpe, M. R. (1993). Leaf export and partitioning changes induced by short-term inhibition of phloem transport. *J. Exp. Bot.* 44, 1491–1496. doi: 10.1093/jxb/44.9.1491

Pritchard, J., Tomos, A. D., Farrar, J. F., Minchin, P. E., Gould, N., Paul, M. J., et al. (2004). Turgor, solute import and growth in maize roots treated with galactose. *Funct. Plant Biol.* 31, 1095–1103. doi: 10.1071/FP04082

Roeb, G. S., and Britz, J. (1991). Short-term fluctuations in the transport of assimilates to the ear of wheat measured with steady-state ^{11}C-CO_2-labelling of the flag leaf. *J. Exp. Bot*. 42, 469–475. doi: 10.1093/jxb/42.4.469

Schmitz, N., Egerton, J. J. G., Lovelock, C. E., and Ball, M. C. (2012). Light-dependent maintenance of hydraulic function in mangrove branches: do xylary chloroplasts play a role in embolism repair? *N. Phytol*. 195, 40–46. doi: 10.1111/j.1469-8137.2012.04187.x

Shackel, K. A., Novelle, V., and Sutter, E. G. (1990). Stomatal Function and cuticular conductance in whole tissue-cultured apple shoots. *J. Am. Soc. Hortic.* 115, 468–472. doi: 10.21273/JASHS.115.3.468

Steppe, K., Saveyn, A., McGuire, M. A., Lemeur, R., and Teskey, R. O. (2007). Resistance to radial CO_2 diffusion contributes to between-tree variation in CO_2 efflux of *Populus deltoides* stems. *Funct. Plant Biol.* 34, 785–792. doi: 10.1071/FP07077

Steppe, K., Sterck, F., and Deslauriers, A. (2015). Diel growth dynamics in tree stems: linking anatomy and ecophysiology. *Trends Plant Sci.* 20, 335–343. doi: 10.1016/j.tplants.2015.03.015

Stringer, J. W., and Kimmerer, T. W. (1993). Refixation of xylem sap CO_2 in *Populus deltoides*. *Physiol. Plant*. 89, 243–251. doi: 10.1034/j.1399-3054.1993.890201.x

Stroock, A. D., Pagay, V. V., Zwieniecki, M. A., and Holbrook, M. N. (2014). The physicochemical hydrodynamics of vascular plants. *Ann. Rev. Fluid Mech.* 46, 615–642. doi: 10.1146/annurev-fluid-010313-141411

Tanner, W., and Beevers, H. (2001). Transpiration, a prerequisite for long-distance transport of minerals in plants? *Proc. Natl. Acad. Sci. U.S.A.* 98, 9443–9447. doi: 10.1073/pnas.161279898

Tarvainen, L., Wallin, G., Lim, H., Linder, S., Oren, R., Ottosson Löfvenius, M., et al. (2017). Photosynthetic refixation varies along the stem and reduces CO_2 efflux in mature boreal *Pinus sylvestris* trees. *Tree Physiol.* 38, 1–12. doi: 10.1093/treephys/tpx130

Teskey, R. O., McGuire, M. A., Bloemen, J., Aubrey, D. P., and Steppe, K. (2017). "Respiration and CO_2 fluxes in trees," in *Plant Respiration: Metabolic Fluxes and Carbon Balance* eds G. Tcherkez, and J. Ghashghaie (Cham: Springer International Publishing), 181–207.

Teskey, R. O., Saveyn, A., Steppe, K., and McGuire, M. A. (2008). Origin, fate and significance of CO_2 in tree stems. *N. Phytol.* 177, 17–32. doi: 10.1111/j.1469-8137.2007.02286.x

Thorpe, M. R., Ferrieri, A. P., Herth, M. M., and Ferrieri, R. A. (2007). ^{11}C-imaging: methyl jasmonate moves in both phloem and xylem, promotes transport of jasmonate, and of photoassimilate even after proton transport is decoupled. *Planta* 226, 541–551. doi: 10.1007/s00425-007-0503-5

Thorpe, M. R., and Minchin, P. E. H. (1991). Continuous monitoring of fluxes of photoassimilate in leaves and whole plants. *J. Exp. Bot.* 42, 461–468. doi: 10.1093/jxb/42.4.461

Thorpe, M. R., Minchin, P. E. H., Williams, J. H. H., Farrar, J. F., and Tomos, A. D. (1993). Carbon import into developing ovules of *Pisum sativum*: the role of the water relations of the seed coat. *J. Exp. Bot.* 44, 937–945. doi: 10.1093/jxb/44.5.937

Troughton, J. H., Chang, F. H., and Currie, B. G. (1974). Estimates of a mean speed of translocation in leaves of *Oryza sativa* L. *Plant Sci. Lett.* 3, 49–54. doi: 10.1016/0304-4211(74)90131-X

Vandegehuchte, M. W., Bloemen, J., Vergeynst, L. L., and Steppe, K. (2015). Woody tissue photosynthesis in trees: salve on the wounds of drought? *N. Phytol.* 208, 998–1002. doi: 10.1111/nph.13599

Wang, Q., Mathews, A. J., Li, K., Wen, J., Komarov, S., O'Sullivan, J. A., et al. (2014). A dedicated high-resolution PET imager for plant sciences. *Phys. Med. Biol.* 59, 5613–5629. doi: 10.1088/0031-9155/59/19/5613

Windt, C. W., Vergeldt, F. J., De Jager, P. A., and Van As, H. (2006). MRI of long-distance water transport: a comparison of the phloem and xylem flow characteristics and dynamics in poplar, castor bean, tomato and tobacco. *Plant Cell Environ.* 29,1715–1729. doi: 10.1111/j.1365-3040.2006.01544.x

Wittmann, C., and Pfanz, H. (2018). More than just CO_2-recycling: corticular photosynthesis as a mechanism to reduce the risk of an energy crisis induced by low oxygen. *N. Phytol.* 219, 551–564. doi: 10.1111/nph.15198

Zeppel, M. J. B., Lewis, J. D., Phillips, N. G., and Tissue, D. T. (2014). Consequences of nocturnal water loss: a synthesis of regulating factors and implications for capacitance, embolism and use in models. *Tree Physiol.* 34, 1047–1055. doi: 10.1093/treephys/tpu089

Conflict of Interest Statement: The authors declare that the research was conducted in the absence of any commercial or financial relationships that could be construed as a potential conflict of interest.

Copyright © 2019 Hubeau, Thorpe, Mincke, Bloemen, Bauweraerts, Minchin, De Schepper, De Vos, Vanhove, Vandenberghe and Steppe. This is an open-access article distributed under the terms of the Creative Commons Attribution License (CC BY). The use, distribution or reproduction in other forums is permitted, provided the original author(s) and the copyright owner(s) are credited and that the original publication in this journal is cited, in accordance with accepted academic practice. No use, distribution or reproduction is permitted which does not comply with these terms.